Topography of the Northern Hemisphere of Mars from the Mars Orbiter Laser Altimeter

D. E. Smith*, M. T. Zuber†, H. V. Frey, J. B. Garvin, J. W. Head, D. O. Muhleman, G. H. Pettengill, R. J. Phillips, S. C. Solomon, H. J. Zwally, W. B. Banerdt, T. C. Duxbury

The first 18 tracks of laser altimeter data across the northern hemisphere of Mars from the Mars Global Surveyor spacecraft show that the planet at latitudes north of 50° is exceptionally flat; slopes and surface roughness increase toward the equator. The polar layered terrain appears to be a thick ice-rich formation with a non-equilibrium planform indicative of ablation near the periphery. Slope relations suggest that the northern Tharsis province was uplifted in the past. A profile across Ares Vallis channel suggests that the discharge through the channel was much greater than previously estimated. The martian atmosphere shows significant 1-micrometer atmospheric opacities, particularly in low-lying areas such as Valles Marineris.

Characterization and modeling of the processes that govern planetary evolution require accurate knowledge of surface topography over a broad range of spatial scales. On 15 September 1997 the Mars Orbiter Laser Altimeter (MOLA) (*1*), an instrument on the Mars Global Surveyor (MGS) spacecraft, acquired its first pass across the surface of Mars. The altimeter obtained measurements of topography (*2*), surface reflectivity (*3*), and backscattered laser pulse width (*4*). This profile was followed by 17 tracks between 14 October and 6 November 1997 that were collected about every 20° of longitude (1200-km separation at the equator) and span from about 80°N to 12°S (*5*) (Fig. 1). The instrument profiled surface features at a maximum vertical resolution of ~30 cm and along-track spatial resolution of 300 to 400 m (*6*).

Before MGS, data sets used to estimate martian topography were Earth-based radar, Mariner 9 and Viking 1 and 2 radio occultations, stereo observations from Mariner 9 and Viking imagery, and the Mariner 9 ultraviolet and infrared spectrometers (*7*). Mariner 9 observations and a model of the gravity field (*8*) were used to define an atmospheric pressure surface of 6.1 mbars as the origin of topography (zero elevation) for Mars. Subsequently, various measurements were combined into digital terrain models (DTMs) (*9*) that were of variable spatial resolution and typically characterized by vertical errors of ~1 to 3 km (*10*). This accuracy and resolution were insufficient for quantitative analysis of the processes that controlled the planet's surface evolution.

Shape and slopes. MOLA topographic profiles (*11*) (Fig. 2) reveal that the northern hemisphere is smooth at the mid- to high latitudes. Elevation and topography increase toward the equator. The mean elevation north of 50°N is about −4 km, and the topography varies by 1773 km. Profiles outside of the vast Tharsis rise (centered at 7°N, 248°E; Passes 24, 26, 33 and 35) are flat or slope gently upward to the south. This low flat area extends across all longitudes and over 2000 km in north-south extent. Over this region the topography along the 17 continuous tracks varies by only ±50 m to ±400 m about a mean sloping surface. The systematic slope (0.056°) from pole to equator is a result of the separation of the center of mass from the center of figure of the planet along the polar axis (*12*) and the ~1-km increase in the mean equatorial radius due to the Tharsis rise. The hemispheric dichotomy boundary region, which separates the low, volcanically and depositionally resurfaced northern hemisphere from the older, heavily cratered and topographically higher southern hemisphere (*13*), has the highest regional slopes. Over baselines of tens of kilometers, slopes are generally 1° to 3°. Local (hundreds of meters) slopes, indicative of surface modification processes and perhaps some relic primary structure, can be steep, and in a few places slopes exceed 20°.

The origin of the flatness of the northern hemisphere is unknown. One explanation of the low elevation of the north relative to the south is that Mars' lithosphere (rigid outer shell) was thinned by regionally vigorous mantle convection or a large impact or impacts (*14*). It has also been suggested that the northern hemisphere was once covered by a vast ocean (*15*). The northern hemisphere of Mars is as smooth as Earth's oceanic abyssal plains, and the volume of water necessary to fill the depression is less than the upper limit of the volume of water estimated for early Mars (*16*). If the water were ~1 km deep, the volume suggested by the MOLA data would be ~15×10^6 km^3. If the water were all transported to the polar regions it would provide enough ice for two polar caps, each 8 km thick and 10° in radius.

Geodesy. A comparison of the planetary radii derived from the MOLA data with the locations of the Viking 1 and 2 and Pathfinder landing sites (*17*) provides a check on the MOLA results. The MOLA data were obtained within about 74 km of the Viking 2 landing site, and the values for the topography at those locations agree to within 260 m. The Viking 1 site is 715 km distant from the nearest MOLA data and the Pathfinder site is 625 km distant. The agreement in topography is ~1000 m in both cases.

The altimeter data have also been compared to the recently re-analyzed occultation measurements obtained on Viking 1 and 2 and Mariner 9. For occultations within 10 km of an altimeter measurement, the difference is −18 ± 118 m, and within 20 km the difference is +34 ± 106 m. Additionally, the altimeter data have been compared with Earth-based radar measurements within 10 km at 34 locations between 10°S and 23°N. For these locations, the MOLA planetary radii are 336 ± 84 m larger than the radar radii.

A comparison of the altimeter spot locations on the surface of Mars with the Mars Digital Image Mosaic (Fig. 1) suggests that the longitudes of features in the images are displaced 10 to 20 km to the east and in some cases to the north or south. The causes of the misalignments are a change in the definition of the prime meridian location of about 0.1°, a possible systematic error in the modeling of the average rotation rate of Mars since Viking, and orbital errors in the original Viking image analyses, each of which can lead to errors of several kilometers.

Polar region. Martian polar deposits play a central role in the cycles of CO_2, H_2O, and dust in the atmosphere. Earlier workers have suggested that the layered terrains were rich in ice (*18*). However, the amount of ice that makes up the layered terrains is

D. E. Smith, H. V. Frey, J. B. Garvin, H. J. Zwally, Earth Sciences Directorate, NASA/Goddard Space Flight Center, Greenbelt, MD 20771, USA.
M. T. Zuber and G. H. Pettengill, Massachusetts Institute of Technology, Cambridge, MA 02139, USA.
J. W. Head, Brown University, Providence, RI 02912, USA.
D. O. Muhleman, California Institute of Technology, Pasadena, CA 91125, USA
R. J. Phillips, Washington University, St. Louis, MO 63130, USA.
S. C. Solomon, Department of Terrestrial Magnetism, Carnegie Institution of Washington, Washington, DC 20015, USA.
W. B. Banerdt and T. C. Duxbury, Jet Propulsion Laboratory, Pasadena, CA 91109, USA.

*To whom correspondence should be addressed.
†Also at: Laboratory for Terrestrial Physics, NASA Goddard Space Flight Center, Greenbelt, MD 20771, USA.

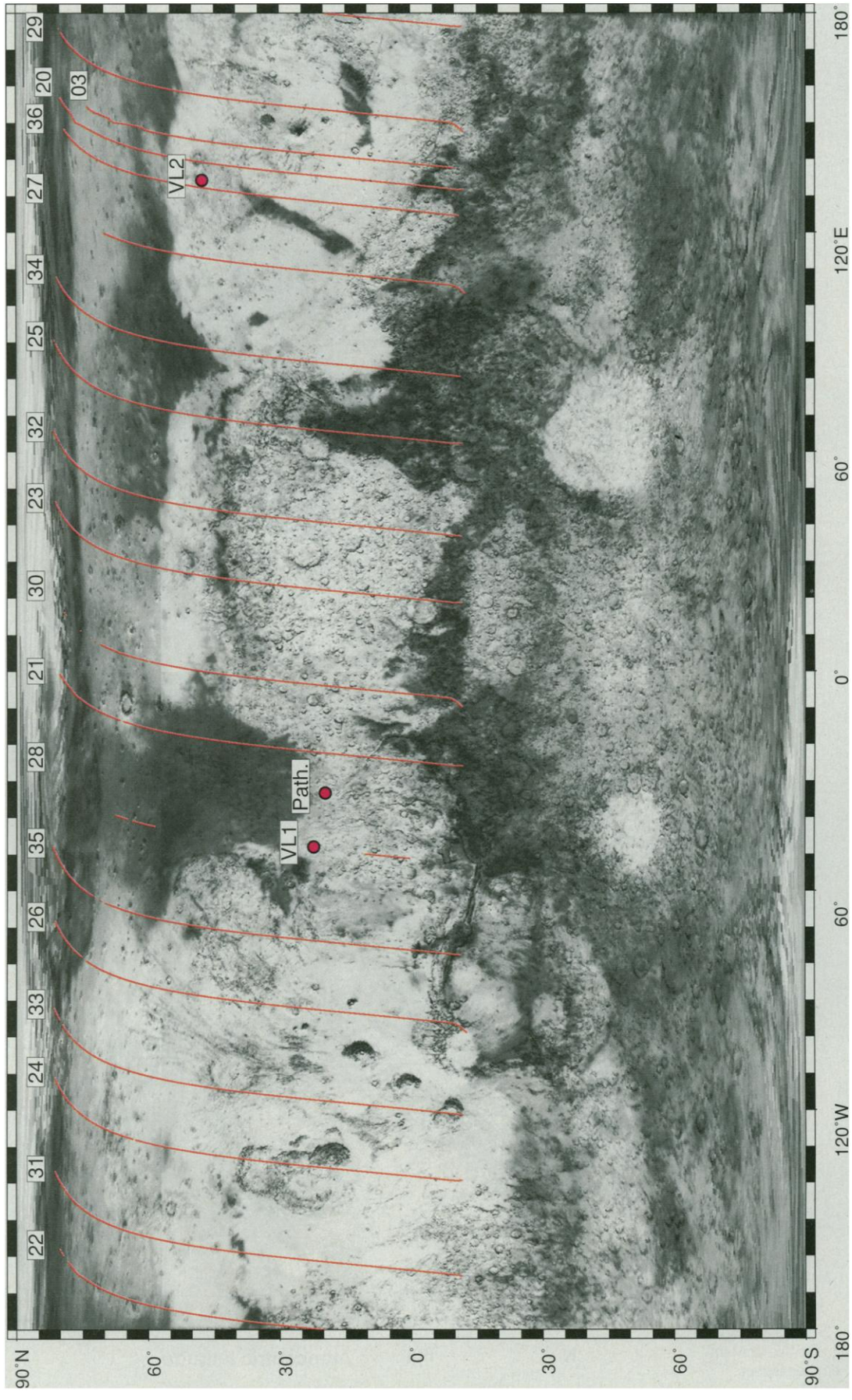

Fig 1. Locations of the MOLA altimeter profiles superimposed on the Mars Digital Photomosaic. Numbers refer to periapse passes of the MGS spacecraft in its elliptical orbit. Shown for comparison are the Viking and Pathfinder landing sites; 1° on Mars at the equator equals ~60 km.

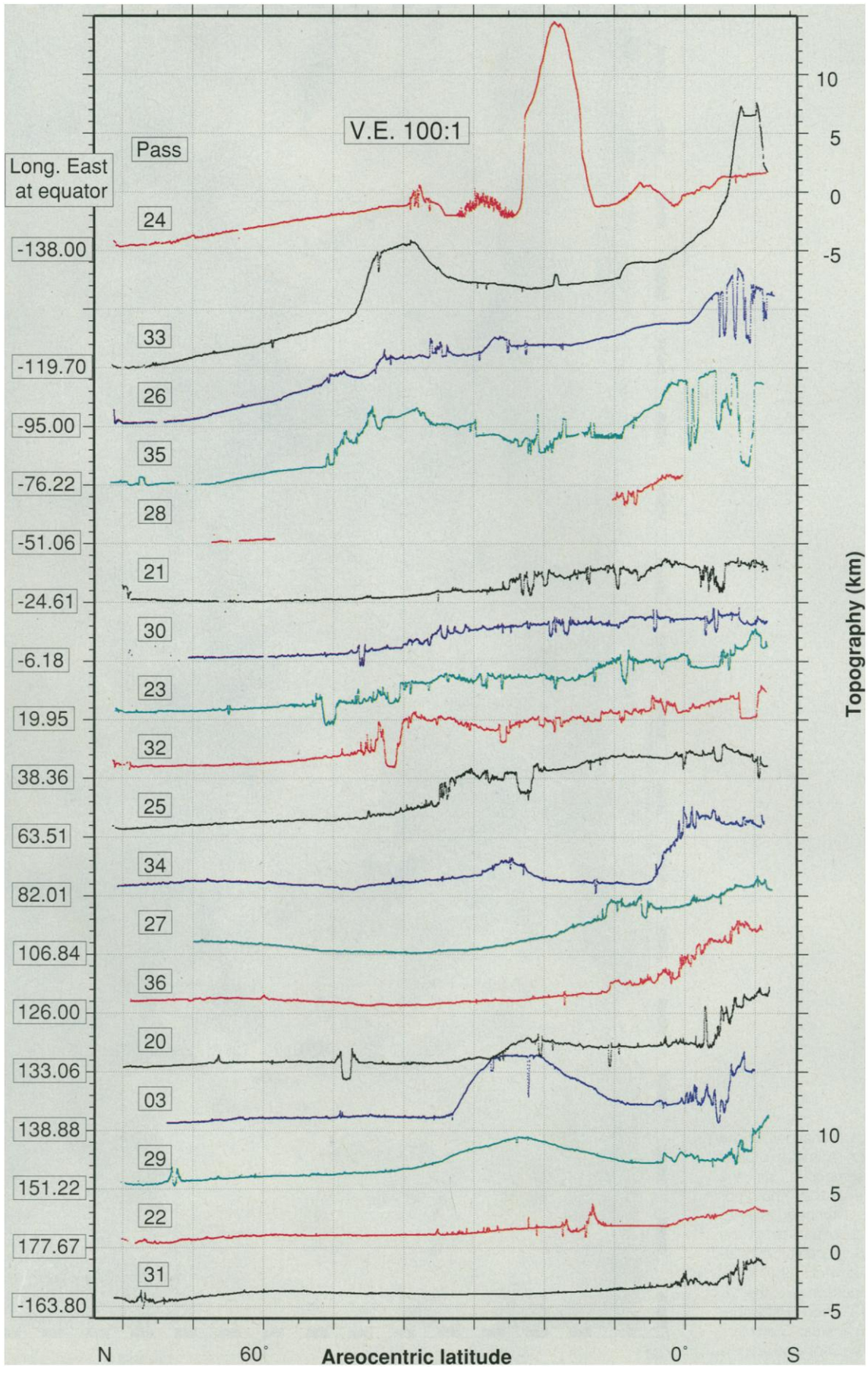

Fig. 2. MOLA topographic profiles of Mars' northern hemisphere.

poorly known, in part because past topographic estimates of the polar deposits had errors of about 1 to 2 km. MOLA measurements of elevation, reflectivity, and pulse width indicate that the layered terrains are composed mainly of ice. Pass 21 (Fig. 3) crossed the layered terrain for ~75 km from 78.8°N to 80.0°N at ~358°E. The elevation rises to 1210 m above the relatively flat dune-covered surface to the south, and crosses two ridges and troughs. The MOLA energy backscattered from the ridges exceeds that of the surroundings by a factor of 3, which indicates ice. The high reflectivity region correlates well with the residual ice field observed by Viking for the summer season. A decrease in reflectivity in the troughs strongly suggests that the ice contains trapped dust. Two other MOLA passes cross layered terrains; in one pass the reflectivity decreased in troughs whereas in the other there was no change. The low elevation and low reflectivities of the Pass 21 troughs support previous suggestions that the troughs are ablation features (*19*). The edge of the layered terrain from the bottom to near the ridge-top is too steep (>15°) to be a steady-state feature and may also be a consequence of ablation. The reflectivity falls off monotonically away from the edge of the layered terrain. One interpretation of this observation is that surface frost extends southward to ~76.5°N. The observed smoothness of the topography on the layered deposits on the scale of hundreds of meters to 1 km, determined from MOLA elevation and pulse-width observations, is consistent with a thick ice cover (*20*).

Impact structures. Impact craters on Mars provide spatially distributed probes of the structure of the shallow planetary interior and the processes that modify the surface. Traditionally, Viking Orbiter imaging data (*21*) were used to describe how the cavity and ejecta blanket shapes of impact craters varied with latitude, terrain type, and relative age. In this study, MOLA traversed 165 craters with diameters ranging from approximately 2 to 150 km. Of these, about 50 were sampled in such a fashion that quantitative measurement of key crater parameters (for example, depth or ejecta thickness) was possible. Figure 4 shows a rampart crater (46°N, 0°E) with a complex ejecta structure that consists of a lobate flow deposit and radial lineations typical of fresh lunar impact craters. At a length scale of 150 m, the root-mean-square (rms) vertical roughness determined by MOLA's return pulse width of the ejecta is greater than that of the crater cavity. This observation is consistent with the expected increase in surface blockiness as the rim crest is approached.

The ratio of the volume of ejecta to that of the apparent cavity (computed under the assumption of axisymmetry) of the crater in Fig. 4 is 1.46 ± 0.05. Values >1 indicate either that infill deposits have reduced the apparent volume of the cavity or that there are unexplained increases in ejecta volume. Over 76 craters had ejecta volume to cavity volume ratios in excess of 1.0. Many of the impact crater ejecta blankets that were observed have variable local slopes and ejecta thickness decay and an apparent volume that is consistent with impact into a fluidized substrate.

Volcanism and tectonics. Mars has volcanic and tectonic structures that preserve the record of the planet's stress and thermal history (*22*). Alba Patera (40.6°N, 250°E) is the largest volcano on Mars (~2700-km diameter) and is characterized by a low profile relative to the other major Tharsis shield volcanoes. A MOLA profile across the western part of Alba (Fig. 5) reveals that its shape is asymmetric in a south to north direction and that this asymmetry is

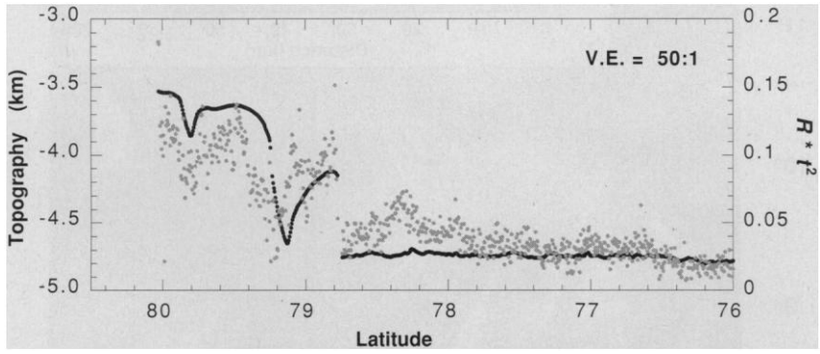

Fig. 3. Topography (in black) and the product of 1.064-μm surface reflectivity times the two-way atmospheric transmission (in gray) of the north polar layered terrain.

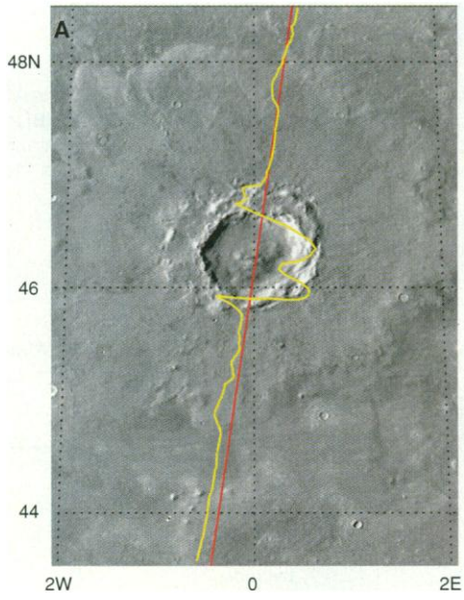

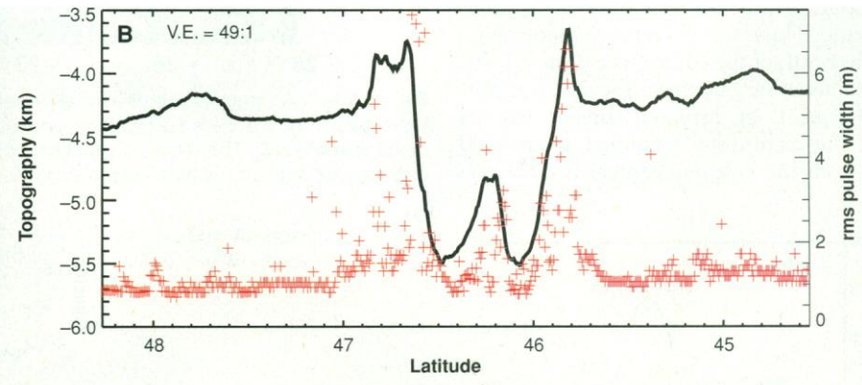

Fig. 4. Topographic profile (in yellow) of a 45-km diameter complex impact crater that displays a lobate ejecta blanket and a central peak. Ramparts at the edge of the ejecta exceed 250 m in relief. The MOLA groundtrack is shown in red. The lower profile shows elevation in black and the backscattered laser pulse width in red.

in part related to the shape of the Tharsis rise on which it sits. The south flank of the volcano has a slope of ~0.77° ± 0.1°, which rolls over to 0.21° ± 0.02° near the 5.7-km-high summit. The northern flank is steeper (1.88° ± 0.1°), and the lower flanks extend for another 800 km to the north at ~0.15° ± 0.02° before intersecting the regional terrain, which has a slope of 0.10° ± 0.01°. The northward-sloping Alba summit approximately parallels (to ~0.1°) the slope of the surrounding terrain north and south of the edifice that forms part of the Tharsis rise. The observed coincidence of slopes suggests that the Alba construct formed before the long wavelength regional topography, and was tilted northward in association with the formation of the Tharsis rise. Removing the regional Tharsis slope (*23*) flattens the Alba summit and makes the north and south flank slopes of the shield more comparable. This observation raises the possibility that regional topography of Tharsis in this area is primarily a consequence of uplift of pre-existing terrain by isostatic or dynamic processes, or intrusive volcanism (*24*), similar to that proposed for the Hawaiian swell (*25*). The relative ages of certain Alba flows (*26*) dictate that surface volcanism (*27*) must also have contributed to the regional elevation. In contrast to Alba, the summit of Arsia Mons is regionally flat, indicating that the main edifice formed after the regional Tharsis topography.

Several topographic depressions are evident on the western flank of Olympus Mons immediately outward of the volcanic edifice. These depressions may reflect subsidence arising from the loading and flexure of the martian lithosphere by the volcano. Estimating the flexural strength of the lithosphere from the topographic profiles outward of the volcano, however, is problematic. There are two relative topographic highs north of the edifice; the nearest (centered about 600 km from the volcano center) consists of disrupted aureole deposits and the more distal (centered about 1200 km from the volcanic center) is older terrain including the densely fractured Acheron Fossae region (*28*). Aureole materials have been attributed to mass movement of slide material from the volcano base (*29*). If the more distal rise originated because of flexure, then a thickness of 75 to 100 km for the underlying elastic lithosphere is implied, and the loading history of Olympus Mons may extend back to the ancient Noachian era. To the south of the edifice, the nearest relative topographic high (centered about 800 km from the volcano center) is within the Medusae Fossae formation, interpreted to be pyroclastic or aeolian deposits (*28*). If this high is flexural in origin, an elastic lithosphere about 40 km thick is implied. The lack of any discernible flexural signatures in the altimetric profiles of Arsia Mons and Alba Patera implies that any flexural depressions must be filled by some combination of volcanic flows and landslide material from the volcano flanks.

Channels. Outflow channels and valley networks on Mars preserve the record of a period when liquid water flowed on the surface (*30*). Estimates of the discharge of these structures provide a basis for constraining the water budget early in the planet's history. In the vicinity of a MOLA pass (orbit 21) across Ares Vallis (Fig. 6), the boundaries of the channel are bordered by terraces that have the same maximum elevation to within about 20 m. We interpret the elevation-paired terraces as marking the

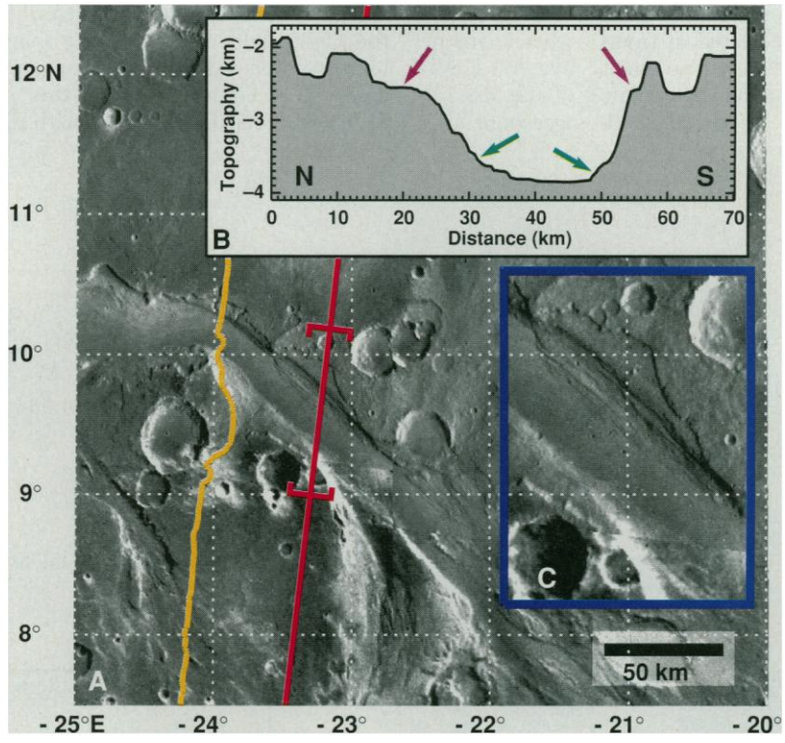

Fig. 6. (**A**) MOLA topographic profile (in yellow) superposed on a Viking Orbiter image mosaic of the Ares Vallis region. The red line is the MOLA groundtrack. Brackets mark elevation segment shown in (**B**) and range of inset in (**C**). This region is ~500 km upstream from the Pathfinder landing site. Magenta and green arrows mark paired terraces and debris flows, respectively. Vertical exaggeration of inset is 11:1.

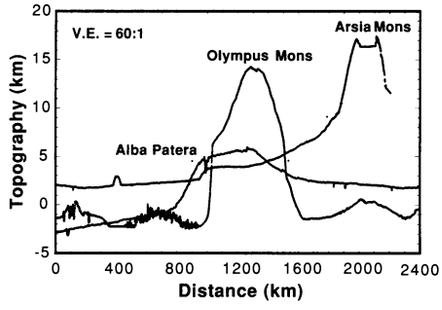

Fig. 5. Topographic profiles of some major volcanic edifices in the Tharsis province.

Fig. 7. Topography (**A**) and derived atmospheric opacity (**B**) over the Ius Chasm of Valles Marineris.

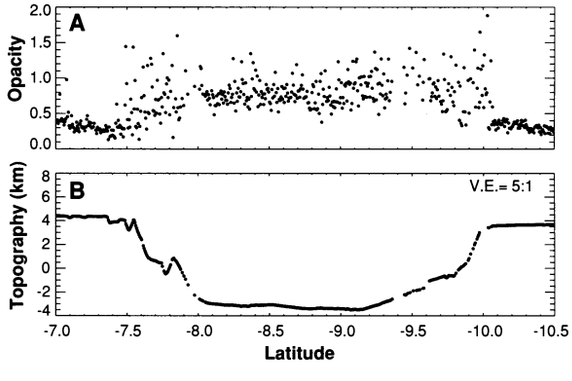

last major flood episode in the channel. In addition there is a second, smaller terrace sitting about 70 m above the dominant north terrace, which may be evidence of an older high-water line. The maximum depth to the channel bottom from the paired terraces is 1300 m, which we take as the water depth for subsequent flow calculations. It is, of course, possible that these terraces formed before the channel flow had incised to its maximum depth. If there were subsequent flows in a more deeply incised channel, they failed to leave behind terraces as evidence. Within the walls of the channel are debris flows (or debris slides) that run out onto the floor of the channel. The well-developed debris flow on the north slope and the dominant north terrace appears to correlate spatially, which provides an alternative interpretation that these terraces were actually water-saturated source regions for the debris flows. If so, then the maximum water depth is still 1300 m unless the debris flows formed after all later episodes of incised flooding.

A previous analysis (*31*) of Ares Vallis yielded estimates of paleoflow conditions on ten cross sections derived from the DTM (*9*). Cross section 10 from this analysis intersects the MGS orbit 21 groundtrack on the north side of the channel and is less than 20 km downstream on the south side. The DTM channel depth is 400 m, whereas the MOLA channel depth using the same elevation reference is at least 1600 m. Given water flow depth and an estimate of slope, we can estimate the inviscid turbulent flow velocity (*32*). Here we follow the same procedures as in (*31*) to show the effects of MOLA data on these earlier analyses; we adopt the critical assumption that flowing water completely filled the observed channel. We estimate that the slope of the channel is 0.002°, the minimum apparent downstream slope found on the south side of the channel, away from the larger debris flow coming off of the north wall. By contrast, Komatsu and Baker (*31*) estimated a slope of 0.02° in this region, which would increase the inferred flow velocity by a factor of 3. Here we obtain a velocity of 142 m s^{-1} (*33*), which is essentially the same as the earlier estimate of 149 m s^{-1}. But the MOLA estimate results from a much different slope as well as channel depth and shape. These differences lead to a discharge estimate of 5×10^9 m^3 s^{-1}, an order of magnitude greater than in (*31*). To obtain the earlier result, the slope must be lowered by a factor of 100, or to 2 cm km^{-1}.

Atmospheric opacity. MOLA also measured the reflected laser energy from the underlying terrain. This quantity can be interpreted as a product of albedo or reflectivity of the surface and two-way atmospheric transmission $e^{-2\tau}$, where τ is total opacity at the 1.064-μm wavelength. We used Viking Orbiter Color Mosaic images as a first-order estimate for the surface albedo and atmospheric opacity (*34*). The calculated opacities for several tracks in the Elysium region (approximate longitude 150°E) rise from 0.4 (L_s = 179°) to 1.0 (L_s = 210°), a range that is consistent with Viking Lander 2 data. We also detected local variations of opacity spanning ~180 km in the region of 60°N–65°N. In such places opacity increased by 1 compared with surroundings, reaching values of 1.5 to 2. We think that such attenuation is due to water ice clouds, which are known to form in the northern part of Mars. Another form of aerosols was detected across Valles Marineris (Fig. 7), where the opacity jumped as the altimeter track crossed into the chasm. We believe that this sudden increase was caused by the presence of afternoon clouds in the canyon, which were also observed by the Mars Orbiter Camera (*35*). Another, less likely, possibility is that the reflected energy decreased because the bottom of the canyon was rough, and this effect was not removed by ratioing with the Viking albedos.

REFERENCES AND NOTES

1. M. T. Zuber *et al.*, *J. Geophys. Res.* **97**, 7781 (1992). The MOLA instrument was designed and built by the Laser Remote Sensing Branch of NASA/GSFC. The laser operated at a wavelength of 1.064 μm, emitting 8-nsec-long pulses with an energy of ~40 mJ at the diode operating temperature during operation in the MGS 35-hour elliptical orbit.
2. MOLA measures the round-trip time of flight of individual laser pulses between the MGS spacecraft and the martian surface. By interpolating the spacecraft orbital trajectory to the time of the laser measurement and correcting for the index of refraction of the martian atmosphere, the one-way light time between the spacecraft and the surface is obtained. Subtraction of the range from the MGS orbit, allowing for off-nadir pointing, yields measurements of martian radius in a center of mass reference frame.
3. Surface reflectivity or albedo at the laser wavelength was determined from the ratio of received to transmitted laser energy. Outgoing pulse energy is sampled with an optical fiber that measures ~95% of the outgoing pulse cross section. The received energy is derived from the area under the curve representing the best estimate of the returned pulse shape. The accuracy of the reflectivity measurement after calibration is ~5%.
4. MOLA's return pulse width provides a measure of the footprint-scale slope or rms roughness of the terrain. The instrument detection electronics contain a bank of four parallel bandpass filters with widths of 20, 60, 180, and 540 nsec that correspond to footprint-scale surface slopes of 1°, 3°, 10°, and 27°. The return pulse triggers the filter that most closely matches the width of the return. Measurement refinement is made using the difference in the times at which the leading and trailing edges of the returned pulse cross the detection threshold. The time difference is translated into an equivalent pulse spread.
5. Ranges were obtained during periapse passes while the MGS spacecraft was at altitudes of ≤786 km above the martian surface. The maximum range was limited by system hardware. Despite non-optimal operating conditions the instrument obtained valid range measurements for ~99% of the output pulses. The laser beam divergence of 400 μrad resulted in a surface spot size of 70 to 300 m.
6. The estimated radial accuracy of the present topography data from MOLA is 30 to 40 m and is dominated by long-wavelength orbital uncertainties of MGS. The precision of the MOLA measurement approaches 30 cm on smooth level surfaces and increases to ~20 m on 30° slopes. The accuracy of the spot location in latitude and longitude is limited by the knowledge of the spacecraft pointing at about 3 mrad (500 to 2000 m on the surface, depending on spacecraft altitude), and spacecraft position uncertainties of several hundred meters.
7. G. S. Downs *et al.*, *J. Geophys. Res.* **87**, 9747 (1982); A. J. Kliore *et al.*, *Icarus* **17**, 484 (1972); G. F. Lindal *et al.*, *J. Geophys. Res.* **84**, 8443 (1979); C. W. Hord, *Icarus* **17**, 443 (1972); B. Conrath *et al.*, *J. Geophys. Res.* **78**, 4267 (1973).
8. J. F. Jordan and J. Lorell, *Icarus* **25**, 146 (1975).
9. R. M. Batson and E. M. Eliason, *Photogram. Eng. Remote Sens.* **61**, 1499 (1995).
10. P. B. Esposito *et al.*, in *Mars*, H. H. Kieffer, B. M. Jakosky, C. W. Snyder, M. S. Matthews, Eds. (Univ. of Arizona Press, Tucson, 1992), p. 209.
11. Topography is defined as the planetary radius minus the radius of the geoid, which is a gravitational equipotential surface. In our analysis we used the geoid from the GMM-1 gravitational field model of Mars [D. E. Smith *et al.*, *J. Geophys. Res.* **98**, 20,871 (1993)], recently recalculated to incorporate up to date IAU geophysical and coordinate system parameters. We define zero elevation using the Mars geoid constrained by the equatorial radius measured by MOLA. The mean equatorial radius of 3396.0 ± 0.3 km represents the average of all elevation measurements within 0.1° latitude of the equator. This is 1.0 km less than the IAU 1991 value and ~2 km larger than previously used in mapping the planet (*9*). The largest contribution to the uncertainty is the sparse data distribution, and the largest source of systematic error is the MGS orbit.
12. D. E. Smith and M. T. Zuber, *Science* **271**, 184 (1996).
13. M. H. Carr, *The Surface of Mars* (Yale Univ. Press, New Haven, 1981).
14. R. E. Lingenfelter and G. Schubert, *Moon* **7**, 172 (1973); D. U. Wise *et al.*, *Icarus* **35**, 456 (1979); D. E. Wilhelms and S. W. Squyres, *Nature* **309**, 138 (1984); H. V. Frey and R. A. Schultz, *Geophys. Res. Lett.* **15**, 229 (1988).
15. V. R. Baker *et al.*, *Nature* **352**, 589 (1991).
16. M. H. Carr *et al.*, *J. Geophys. Res.* **78**, 4049 (1973); R. Greeley, *Science* **236**, 1653 (1987); V. R. Baker *et al.*, in *Mars*, H. H. Kieffer, B. M. Jakosky, C. W. Snyder, M. S. Matthews, Eds. (Univ. of Arizona Press, Tucson, 1992), p. 493.
17. W. M. Folkner *et al.*, *Science* **278**, 1749 (1997).
18. P. Thomas *et al.*, in *Mars*, H. H. Kieffer, B. M. Jakosky, C. W. Snyder, M. S. Matthews, Eds. (Univ. of Arizona Press, Tucson, 1992), p. 767; M. C. Malin, *Geophys. Res. Lett.* **13**, 444 (1986). D. A. Paige *et al.*, *J. Geophys. Res.* **99**, 25,595 (1994).
19. A. D. Howard *et al.*, *Icarus* **50**, 245 (1982); K. R. Blasius *et al.*, *ibid.*, p. 140.
20. We apply a steady-state mass balance model [W. F. Budd *et al.*, *Polarforschung* **56**, 43 (1986)] for the shape of the layered terrains and assume that the rheology is perfectly plastic. A first-order approximation for the ice surface elevation profile is a parabola with ice thickness h where $h = [2\,\tau_0(L - x/\rho\, g)^{1/2}]$, and L is the radius of the cap (= 675 km), x is the distance from the center, τ_0 is yield stress, ρ is density, and g (3.7 m s^{-2}) is the acceleration of gravity. The model, which assumes no basal sliding, correctly predicts the 3200-m height of the Greenland ice sheet. For pure H_2O ice (τ_0 = 100 kPa; ρ = 910 kg m^{-3}) the model suggests that the ice at the martian north pole could conceivably achieve a thickness of up to 5 km. For pure CO_2 ice (τ_0 = 10 MPa; ρ = 1589 kg m^{-3}) a cap thickness of ~40 km at the pole would be expected. While more detailed rheological modeling is required, these results favor an H_2O-dominated composition.
21. M. H. Carr *et al.*, *J. Geophys. Res.* **82**, 4055 (1977);

D. J. Jankowski and S. W. Squyres, *Icarus* **100**, 26 (1992).
22. P. J. Mouginis-Mark *et al.*, in *Mars*, H. H. Kieffer, B. M. Jakosky, C. W. Snyder, M. S. Matthews, Eds. (Univ. of Arizona Press, Tucson, 1992), p. 424; W. B. Banerdt *et al.*, *ibid.*, p. 249; G. Schubert *et al.*, *ibid.*, p. 147.
23. M. T. Zuber and D. E. Smith, *J. Geophys. Res.*, **102**, 28,673 (1997).
24. R. J. Phillips *et al.*, *ibid.* **95**, 5089 (1990).
25. J. Phipps Morgan *et al.*, *ibid.* **100**, 8045 (1995).
26. K. L. Tanaka *et al.*, in *Mars*, H. H. Kieffer, B. M. Jakosky, C. W. Snyder, M. S. Matthews, Eds. (Univ. of Arizona Press, Tucson, 1992), p. 345.
27. S. C. Solomon and J. W. Head, *J. Geophys. Res.* **82**, 9755 (1982).
28. D. H. Scott and K. L. Tanaka, *U.S. Geol. Survey Map I-1802-A* (1986).
29. R. M. C. Lopes *et al.*, *Moon Planets* **22**, 221 (1980); P. W. Francis and G. Wadge, *J. Geophys. Res.* **88**, 8333 (1983).
30. M. H. Carr, *Water on Mars* (Oxford Univ. Press, New York, 1996).
31. G. Komatsu and V. R. Baker, *J. Geophys. Res.* **102**, 4151 (1997).
32. We use the Chezy equations [R. A. Granger, *Fluid Mechanics* (Dover, New York, 1995)] to estimate average flow velocity; v, is given by $v = C(Rs)^{1/2}$, where C is the Chezy coefficient, s is local slope, and R is hydraulic radius, defined as the ratio of flow cross-sectional area to perimeter of the wetted channel. In SI units, $C = (1/n)R^{1/6}$, where n is the Manning roughness coefficient, here square-root-gravity scaled from an assumed terrestrial value of 0.02. Hydraulic radius is obtained directly from MOLA data, assuming that the water level reached the paired-terraces and attempting to adjust the channel perimeter for post-flow mass wasting. A more difficult problem is estimation of slope. In principle, the apparent slope measured along the groundtrack can be projected into the downstream direction to yield true channel slope. The orbital track makes an angle of 50° with the downstream vector and true slope = apparent slope/cos(50°). The presence of debris flows on the channel floor could locally modify this slope.
33. This velocity and the channel depth of 1300 m yield a Froude number [$Fr = V/(hg)^{1/2}$, where h is channel depth and g is gravity] of 2.0. This value indicates supercritical flow.
34. The filter of the Viking Orbiter Camera nearest to the MOLA wavelength is red [0.5 μm to 0.7 μm; M. H. Carr *et al.*, *Icarus* **16**, 17 (1972)]. We have adopted a scaling factor of 0.8 to convert those images to 1.064 μm to be consistent with spectroscopic observations of the average martian surface in visible and infrared wavelengths [L. A. Soderblom, in *Mars*, H. H. Kieffer, B. M. Jakosky, C. W. Snyder, M. S. Matthews, Eds. (Univ. of Arizona Press, Tucson, 1992), p. 557]. It is not possible to obtain unbiased values of opacity using the above method, because the Viking images are not themselves corrected for the relevant atmospheric opacity. We used only Viking images that exhibited little or no obscuration. Such opacities in the Viking images may either darken or brighten them, unlike the effect in MOLA reflectivities, which is pure extinction. We estimated that average Viking images were darkened with an opacity of 0.4 and added this to the MOLA opacities.
35. M. C. Malin *et al.*, *Science* **279**, 1681 (1998).
36. We thank MOLA Instrument Manager R. Follas and the rest of the instrument team, and G. Cunningham, B. McAnally, and the MGS spacecraft and operation teams. We also acknowledge helpful reviews from M. Carr and an anonymous reviewer, and contributions from J. Abshire and J. Smith in instrument calibration and performance assessment, G. Neumann, G. Elman, P. Jester, and J. Schott in altimetry processing, F. Lemoine, D. Rowlands, and S. Fricke in orbit determination, and O. Aharonson, D. Brown, J. Frawley, P. Haggerty, S. Hauk, A. Ivanov, P. McGovern, C. Johnson, S. Pratt, and N. Siebert in analysis. The MOLA investigation is supported by the NASA Mars Global Surveyor Project.

15 January 1998; accepted 19 February 1998

Results from the Mars Global Surveyor Thermal Emission Spectrometer

P. R. Christensen,* D. L. Anderson, S. C. Chase, R. T. Clancy, R. N. Clark, B. J. Conrath, H. H. Kieffer, R. O. Kuzmin, M. C. Malin, J. C. Pearl, T. L. Roush, M. D. Smith

The Thermal Emission Spectrometer spectra of low albedo surface materials suggests that a four to one mixture of pyroxene to plagioclase, together with about a 35 percent dust component provides the best fit to the spectrum. Qualitative upper limits can be placed on the concentration of carbonates (<10 percent), olivine (<10 percent), clay minerals (<20 percent), and quartz (<5 percent) in the limited regions observed. Limb observations in the northern hemisphere reveal low-lying dust hazes and detached water-ice clouds at altitudes up to 55 kilometers. At an aerocentric longitude of 224° a major dust storm developed in the Noachis Terra region. The south polar cap retreat was similar to that observed by Viking.

The Thermal Emission Spectrometer (TES) investigation is designed to study the surface and atmosphere of Mars using thermal infrared (IR) spectroscopy, together with broadband thermal and solar reflectance radiometry. These observations will build upon IR observations collected by previous spacecraft, in particular the Mariner 9 Infrared Interferometer Spectrometer (IRIS) (*1*, *2*) and Viking Infrared Thermal Mapper (IRTM) investigations (*3*, *4*).

The specific objectives of the TES experiment are: (i) to determine and map the composition of surface minerals, rocks, and ices; (ii) to study the composition, particle size, and spatial and temporal distribution of atmospheric dust; (iii) to locate water-ice and CO_2 condensate clouds and determine their temperature, height, and condensate abundance; (iv) to study the growth, retreat, and total energy balance of the polar cap deposits; (v) to measure the thermophysical properties of the martian surface materials; and (vi) to characterize the thermal structure and dynamics of the atmosphere (*5*).

The TES instrument consists of three subsections: (i) a Michelson interferometer that collects spectra from 1700 to 200 cm^{-1} (~6 to 50 μm) at either 5 or 10 cm^{-1} spectral resolution, (ii) a bore-sighted bolometric thermal radiance spectrometer (4.5 to ~100 μm), and (iii) a solar reflectance spectrometer (0.3 to 2.7 μm). The TES has a noise equivalent spectral radiance near 1.2×10^{-8} W^{-1} cm^{-2} str^{-1} cm^{-1}. This corresponds to a signal-to-noise ratio (SNR) of 490 at 1000 cm^{-1} (10 μm) viewing a 270 K scene. Absolute radiometric accuracy was estimated from pre-launch data to be about 4×10^{-8} W^{-1} cm^{-2} str^{-1} cm^{-1}. However, in-flight observations indicated that a small, systematic calibration offset of $\sim 1 \times 10^{-7}$ W^{-1} cm^{-2} str^{-1} cm^{-1} is present in the TES data. This error is primarily due to slight variations in the instrument background energy between observations taken of space for calibration and those viewing the planet at an angle 90° away (*6*).

The data presented here were collected between 14 September and 30 November 1997, corresponding to orbits 2 to 53 and covering the southern spring season from aerocentric longitude (L_s) 182° to 228°. Throughout this period Mars Global Surveyer (MGS) was in a highly elliptical orbit such that the spatial resolution and observation angular velocity varied widely (*7*). During each periapsis pass the TES pointing mirror is pointed as close to nadir as possible, resulting in observations with emission angles between 0° and 30°. The spatial resolution at periapsis is as low as 1 km in

P. R. Christensen and D. L. Anderson, Arizona State University, Tempe, AZ 85287, USA.
S. C. Chase, Santa Barbara Remote Sensing, Goleta, CA 93017, USA.
R. T. Clancy, University of Colorado, Boulder, CO 80309, USA.
R. N. Clark, U.S. Geological Survey, Denver, CO 80225, USA.
B. J. Conrath, Cornell University, Ithaca, NY 14850, USA.
H. H. Kieffer, U.S. Geological Survey, Flagstaff, AZ 86001, USA.
R. O. Kuzmin, Vernadsky Institute, Moscow, Russia.
M. C. Malin, Malin Space Science Systems, San Diego, CA 92121, USA.
J. C. Pearl and M. D. Smith, Goddard Space Flight Center, Greenbelt, MD 20771, USA.
T. L. Roush, Ames Research Center, Moffet Field, CA 94035, USA.

*To whom correspondence should be addressed. E-mail: phil.christensen@asu.edu